JOURNAL OF THERMOPHYSICS AND HEAT TRANSFER
Vol. 13, No. 3, July–September 1999

Impingement Cooling in Rotating Two-Pass Rectangular Channels with Ribbed Walls

Kumar V. Akella* and Je-Chin Han†
Texas A&M University, College Station, Texas 77843-3123

Impingement cooling was studied on ribbed walls in rotating two-pass rectangular channels with a sharp 180-deg turn. Two rows of circular jets impinged opposite to the direction of rotation in one channel and in the same direction of rotation in the other channel. Square cross-sectioned ribs were periodically attached to the target walls and inclined at a 45-deg angle to the direction of spent airflow. Rib pitch to height and rib height to channel hydraulic diameter ratios were fixed at 10 and 0.125, respectively. After impingement, spent air (crossflow) traveled radially outward and inward in the first and the second impingement channel, respectively. Jet Reynolds numbers and rotation numbers varied from 4×10^3 to 1×10^4 and 0 to 0.0133, respectively. As the jet Reynolds number increased from 4×10^3 to 1×10^4, the ratios of channel-averaged ribbed to smooth surface Nusselt numbers increased from 13 to 47% for the nonrotating test. For the rotating test, however, these ratios changed from 9 to 44% as the jet Reynolds number increased. Rotation-induced Coriolis and centrifugal forces altered the pressure distribution, but the jet velocity distribution was not significantly affected. However, those rotation-induced forces decreased the Nusselt number values up to 20% in the ribbed impingement channels.

Nomenclature

A_f	= ratio of total area of jets impinging on a copper plate to area of heated copper plate (open area ratio), $n\pi d_j^2/(4A_w)$
A_w	= area of copper plate (rib-increased surface area not included)
D_h	= hydraulic diameter of the impingement channel
d_j	= diameter of the impinging jet
e	= rib height
$F_{c,\mathrm{Cor}}$	= channel crossflow Coriolis force, $\rho\Omega V_c$
F_{cen}	= centrifugal force, $\rho\Omega^2 r$
$F_{j,\mathrm{Cor}}$	= jet Coriolis force, $\rho\Omega V_j$
G_c	= channel crossflow mass flux, ρV_c
G_j	= jet mass flux, ρV_j
h	= regionally averaged heat transfer coefficient on each copper plate
k	= thermal conductivity of air (coolant)
L	= length of the test model
m_j	= jet mass flow rate
Nu	= regionally averaged Nusselt number on each copper plate for the rotating test
Nu_{av}	= channel-averaged (first or second) Nusselt number for the rotating test
Nu_0	= regionally averaged Nusselt number on each copper plate for the nonrotating test
$Nu_{0,\mathrm{av}}$	= channel-averaged (first or second) Nusselt number for the nonrotating test
n	= number of jets impinging on a copper plate
p	= rib pitch
q_{loss}	= heat conducted to the test stand from copper plates
q_{total}	= total heat input to the copper plates
Re_j	= channel-averaged jet Reynolds number, $\rho V_{j,\mathrm{av}} d_j/\mu$
R_m	= mean rotating radius of the test model
Ro	= channel-averaged jet rotation number, $\Omega d_j/V_{j,\mathrm{av}}$
r	= radial location in the supply and impingement channels from the center of rotation
T_b	= measured air temperature in impingement channels
T_f	= film temperature, $(T_w + T_b)/2.0$
T_j	= air (coolant) temperature measured at the inlet of the first supply channel
T_w	= regionally averaged copper plate (wall) temperature
$T_{w,\mathrm{av}}$	= channel-averaged copper plate (wall) temperature
$(T_{w,\mathrm{av}} - T_j)/T_{w,\mathrm{av}}$	= ratio of wall to air temperature difference to wall temperature, °R
V_c	= channel crossflow velocity
V_j	= jet velocity
$V_{j,\mathrm{av}}$	= channel-averaged jet velocity
X	= radial location of wall and air temperature measurements in the impingement channels from the inlet of the first impingement channel
X_n	= streamwise distance between adjacent jet holes
Y_n	= spanwise distance between jet holes
Z_n	= distance between the jet plate and copper plates in the impingement channels
α	= angle between the rib and direction of crossflow (rib-orientation angle), 45 deg
μ	= dynamic viscosity of air (coolant)
ρ	= density of air (coolant)
Ω	= rotation speed of test model, rpm

Introduction

SEVERAL investigators have conducted heat transfer experiments in impingement channels in nonrotating blades. Kercher and Tabakoff,[1] Chance,[2] and Florschuetz et al.[3] studied the effects of jet geometry (d_j, X_n, Y_n, Z_n, and A_f), flow parameters (Re_j, V_j, and G_c/G_j), and thermal conditions [$(T_{w,\mathrm{av}} - T_j)/T_{w,\mathrm{av}}$]. They found that, for a given jet configuration, impingement heat transfer increases with increasing jet Reynolds number Re_j but decreases with increasing spent air crossflow (G_c/G_j). Van Treuren et al.[4] and

Received 31 August 1998; revision received 11 February 1999; accepted for publication 12 February 1999.

*Graduate Research Assistant, Department of Mechanical Engineering.
†HTRI Professor, Department of Mechanical Engineering. Associate Fellow AIAA.

Huang et al.[5] measured local heat transfer values with unrestricted (minimum) crossflow and various exit flow orientations, respectively. Trabold and Obot[6] studied impingement heat transfer on ribbed walls (rib-orientation angle of 90 deg) with intermediate and maximum crossflow schemes. Geometry (X_n, Y_n, Z_n, A_f, and p/e) and flow parameters (Re_j, V_j, and G_c/G_j) were varied. Ribs resulted in small reductions in the heat transfer coefficient in the upstream section, but improvements in heat transfer were observed in the downstream section for the maximum crossflow scheme. Gau and Lee[7] studied flow structure and heat transfer along ribbed walls (rib-orientation angle of 90 deg) from a single slot air jet. Rib pitch to height ratio, slot width to rib height ratio, and nozzle to target wall spacing varied in the investigation. Studies[6,7] concluded that ribs could compensate for the degradation of the heat transfer that is usually associated with the crossflow. Haiping et al.[8] measured impingement heat transfer values on a ribbed wall (rib-orientation angle of 90 deg) for various values of initial crossflow approaching the impingement channel. Four different cases of jet position with respect to rib position were considered: 1) jet directed before the rib, $-p/4$; 2) jet directed on the rib, $p = 0$; 3) jet directed behind the rib, $p/4$; and 4) jet directed midway between the ribs, $p/2$. Haiping et al.[8] concluded that higher heat transfer values are obtained with jets impinging midway between the ribs, when compared with the other three cases.

Rotating blades experience large Coriolis and centrifugal buoyancy forces. These forces produce strong secondary flows and alter the flow and heat transfer profiles in impingement channels. Few investigators have studied the combined effects of Coriolis and buoyancy forces on impingement cooling. Epstein et al.[9] studied the effects of flow (Re_j and Ro) and buoyancy in the leading edge of an airfoil from a single row of circular jets. Heat transfer values were presented for two model orientations: 1) the angle (stagger angle) between the jet direction and direction of rotation is 90 deg and 2) stagger angle is 60 deg. Buoyancy forces decreased the Nusselt number values 25% when compared with nonrotating values. Mattern and Hennecke[10] used the naphthalene sublimation technique to study the effects of jet geometry (Y_n/d_j and Z_n/d_j), flow (Re_j and Ro), and stagger angle (0, 15, 30, 45, 75, and 90 deg) on the local heat/mass transfer values. This study only considered the Coriolis force effect on heat/mass transfer distribution. The buoyancy force effect on heat/mass transfer was not included. Measurements were obtained in the leading edge on an airfoil from a single row of circular jets. Rotation reduced the heat transfer values between 10 and 40%, according to the stagger angle.

Studies[11,12] investigated impingement cooling in the midchord region of a rotating blade, from an inline array of circular jets. Parsons et al.[11] measured heat transfer values in single-pass rectangular channels and reported that rotation decreased the Nusselt number values 20% compared with nonrotating values. Akella and Han[12] studied impingement cooling in two-pass rectangular channels, with the channels connected by a sharp 180-deg turn. Rotation decreased the Nusselt number values 20 and 25% below the nonrotating values in the impingement channels and the turn region, respectively. Also, Nusselt number values in the turn region were 60% higher when compared with the values in the impingement channels for higher jet flow rates and over the range of rotation speeds tested. Studies[9–12] focused on the effects of rotation in impingement-cooled channels with smooth walls.

Secondary flows produced by angled ribs and rotation interact with each other and develop a new heat transfer pattern that is different from those produced by angled ribs or by rotation alone. Relevant studies on convection cooling in rotating channels with angled ribs are cited here. Johnson et al.[13] conducted experiments to determine the effects of buoyancy and Coriolis forces in serpentine ribbed channels. A rib-orientation angle of 45 deg was maintained on the leading and trailing surfaces of the rotating channel. Johnson et al. concluded that angled ribs (45 deg) provided 10–30% greater heat transfer coefficients when compared with normal ribs (90 deg). Zhang et al.[14] studied the influence of rotation on heat transfer in a two-pass channel with ribbed walls. Angled ribs (60 deg) were applied on both the leading and trailing walls of the rotating channel. Angled ribs, besides tripping the boundary layer, produce a secondary flow pattern that increases the heat transfer from the surfaces. Therefore, most of the increases in heat transfer with angled ribs, when compared with those with normal ribs, are attributed to changes in the flow characteristics. Johnson et al.[13] and Zhang et al.[14] concluded that angled ribs generate secondary flow and produce greater heat transfer coefficients than normal ribs (90 deg) for both nonrotating and rotating blades.

These studies[9–14] have not addressed the following issues on impingement heat transfer: 1) the effect of angled ribs in nonrotating impingement-cooled blades and 2) the combined effect of rotation and angled ribs in rotating impingement-cooled blades. The compound heat transfer enhancement technique, such as impingement and angled ribs, may provide a better cooling effect for high-temperature gas turbine blades compared to those with impingement cooling or angled rib cooling alone. This study measured flow and heat transfer in an impingement-cooled rotating blade with angled ribs on its inner surfaces. Square cross-sectioned ribs with a rib-orientation angle of 45 deg were applied to the target walls. Measurements were obtained in a two-pass rectangular impingement channel, with the channels connected by a sharp 180-deg turn. The effect of the jet direction with respect to the rotation direction was also addressed.

Experimental Apparatus

The schematic of the test model is shown in Fig. 1. Akella and Han[12] discussed most of the test model construction; however, the test model was modified to conduct the current investigation. The aspect ratio and the hydraulic diameter of the supply and the impingement channel are 0.5 and 12.71 mm. Two rows of

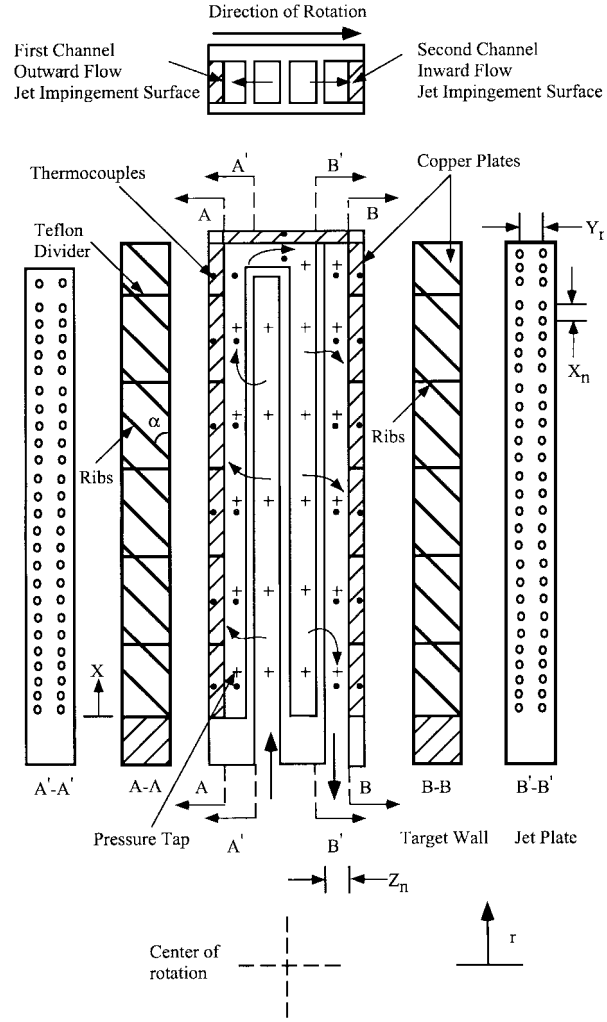

Fig. 1 Schematic of test model.

circular jets impinged on the copper plates in the first and second impingement channels. Spent air (crossflow) moved radially outward and inward, in the first and second impingement channels, respectively. The dimensions of copper plates in the impingement channels and the turn region are $34.93 \times 19.05 \times 3.18$ mm^3 and $44.45 \times 19.05 \times 3.18$ mm^3, respectively. However, the dimensions of the copper plates just upstream and downstream of the turn region are $25.40 \times 19.05 \times 3.18$ mm^3. Most of the impingement channels had 10 jets impinged on each copper plate, whereas the number of jets impinging upstream and downstream of the turn region are 2 and 6, respectively. The dimensions of the test model are 1) d_j and thickness of the jet plate, t, fixed at 3.18 mm and $0.5d_j$, respectively; 2) X_n, Y_n, and Z_n fixed at $2d_j$, $3d_j$, and $3d_j$, respectively; and 3) A_f, R_m, and L fixed at 12%, $197d_j$, and $86d_j$, respectively. Square cross-sectioned brass ribs are periodically attached to the target walls with a two-part epoxy 907 adhesive compound. The adhesive thickness was less than 0.1 mm, which resulted in a negligible thermal insulation effect between the ribs and copper plates. The geometric parameters of the ribs are α, e, p, and D_h fixed at 45 deg, 1.59 mm, $10e$, and $8e$, respectively.

Pressure distribution was measured and local jet velocities were calculated under adiabatic wall conditions at various radial locations. The impingement channels and turn region were heated separately by resistance heaters coated with polyester. The heaters were uniformly cemented in the grooves behind the copper plates. This created a nearly uniform wall heat flux boundary condition. Teflon® insulation of 1.59-mm thickness reduced the heat conduction between adjacent copper plates. T-type thermocouples, as shown in Fig. 1, embedded behind the copper plates (at 13 different locations) and in the impingement channels (at 13 different positions), measured the regionally averaged wall and air temperatures, respectively.

The schematic of the rotating impingement test stand is shown in Fig. 2. The test stand construction is similar to the one discussed in Ref. 12. A brief description of the test stand follows. The test model is mounted at one end of the rotating arm with the other end of the arm acting as a counterbalance. Thermocouple readings to the data logger and power to the resistance heaters were transferred by a 100-channel slip ring unit. A 48-port scanivalve unit mounted on top of the slip ring unit recorded pressure measurements. One port was connected to a u-tube manometer for the pressure transducer calibration. An electric motor rotated the test model, slip ring unit, and scanivalve.

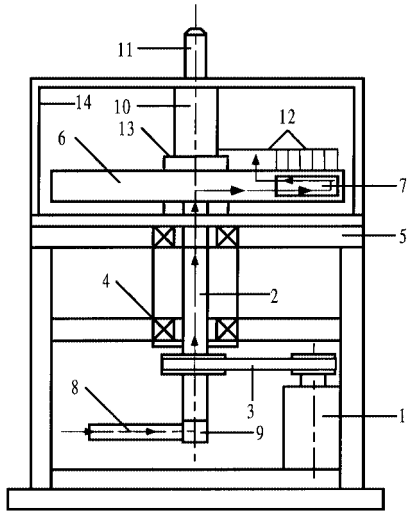

1.	Electric Motor	8.	Compressed Air
2.	Rotating Shaft	9.	Rotating Union
3.	Belt Drive	10.	Slip Ring Unit
4.	Bearing Support	11.	Scanivalve Unit
5.	Steel Table	12.	Pressure Taps
6.	Rotating Arm	13.	Hub
7.	Test Model	14.	Safety Guard

Fig. 2 Schematic of rotating impingement test stand.

Experimental Procedure and Data Analysis

The pressure distribution, jet mass flow rates, and velocities were assumed to be independent of temperature. Local jet mass flow rates and velocities were estimated from the pressure measurements,

$$m_j = Sd_j^2 C_d \sqrt{(P_s/T_j)(P_s - P_i)} \tag{1}$$

$$V_j = \frac{4m_j}{n\rho_j \pi d_j^2} \tag{2}$$

where S is a constant, 0.052; C_d is the channel-averaged jet discharged coefficient; P_s is pressure in the supply channel; and P_i is pressure in the impingement channel. C_d was calculated to be in the range of 0.65–0.67 from the overall mass balance in the test model.[12] The uncertainty in the pressure transducer measurements, m_j, and V_j, were ± 0.15, ± 2.5 and ± 4.0%, respectively.

Heat loss was estimated by running a separate experiment on the same test model at various temperature levels, but without air in the test model. The heat lost from each copper plate to the surroundings was calculated as

$$q_{\text{loss}} = A + B(T_w - T_{\text{amb}}) \tag{3}$$

Heat loss power q_{loss} was calculated as a function of temperature difference between the copper plate and the surroundings. A and B are constants evaluated for each copper plate at all of the rotation speeds tested and T_{amb} is the surrounding (laboratory) air temperature. The heat loss power to total power input increased from 15 to 25% as the rotation speed increased from 0 to 800 rpm at $Re_j = 4 \times 10^3$. However, at high Reynolds number ($Re_j = 1 \times 10^4$), these ratios increased from 10 to 17% as the rotation speed increased. At low Reynolds number, conduction between adjacent copper plates was less than 2% of the total power input.

Bulk temperatures T_b were measured adjacent to the copper plates in the impingement channels and the turn region. The measured values of T_b were compared with the energy balance values and were within ± 10% for all jet Reynolds numbers and rotation speeds tested. Also, $(q_{\text{total}} - q_{\text{loss}})$ was the net heat input carried away by the jets and crossflow from each copper plate. The heat transfer coefficient h was calculated based on thermocouple measurements of wall and air temperatures,

$$h = \frac{(q_{\text{total}} - q_{\text{loss}})}{A_w(T_w - T_b)} \tag{4}$$

where A_w is the area of copper plate (665.42 mm^2) in the impingement channel. In the calculations of the heat transfer coefficient, the rib-increased surface area (185.62 mm^2 on each copper plate) is not included in the analysis. According to Kline and McClintock,[15] the uncertainty in the measurement of mass flow rate, jet Reynolds number, and Nusselt number at $Re_j = 4 \times 10^3$ was ± 6, ± 7, and ± 10%, respectively. However, these values decreased to ± 3, ± 4, and ± 6%, respectively, at $Re_j = 1 \times 10^4$.

Experimental Results and Discussion

Some of the important parameters influencing impingement cooling are 1) geometry (d_j, X_n/d_j, Y_n/d_j, Z_n/d_j, R_m/d_j, and A_f), 2) flow rate (Re_j), 3) rotation speed (Ro), 4) direction of impingement with respect to rotation direction, 5) direction of channel crossflow, 6) surface roughness (α, e, p/e, and e/D_h), and 7) thermal boundary conditions.

The test parameters for this investigation are 1) fixed geometric parameters; 2) $Re_j = 4 \times 10^3$, 6×10^3, 8×10^3, and 1×10^4; 3) $\Omega = 0$, 400, and 800 rpm; 4) forward and reverse direction of rotation; 5) radially outward and inward in the first and second impingement channel, respectively; 6) fixed roughness parameters; and 7) uniform wall heat flux boundary condition or $(T_{w,\text{av}} - T_j)/T_{w,\text{av}} = 0.083$ and 0.07 for 0 and 800 rpm, respectively. Electric heat was only applied to the impingement target wall; the other three walls were not heated. Average surface temperatures $T_{w,\text{av}}$ for the first pass six copper plates and for the second pass six copper plates

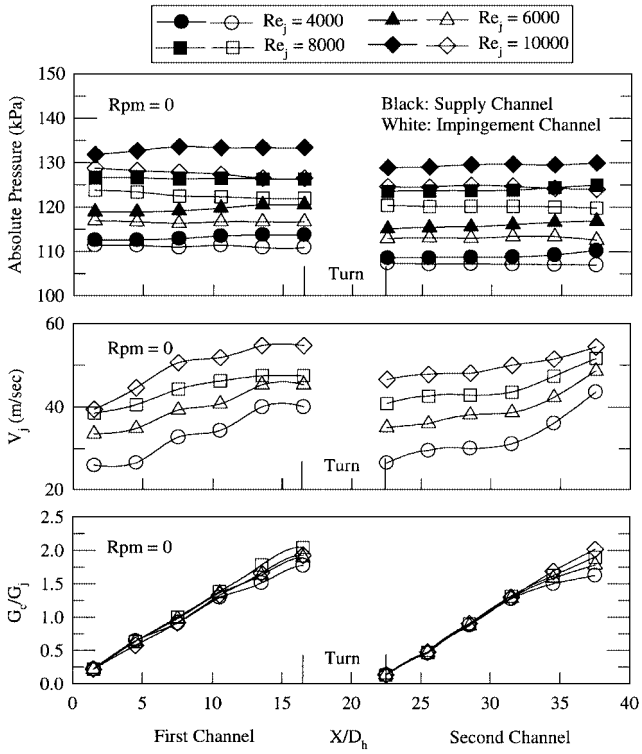

Fig. 3 Flow distribution for nonrotating test.

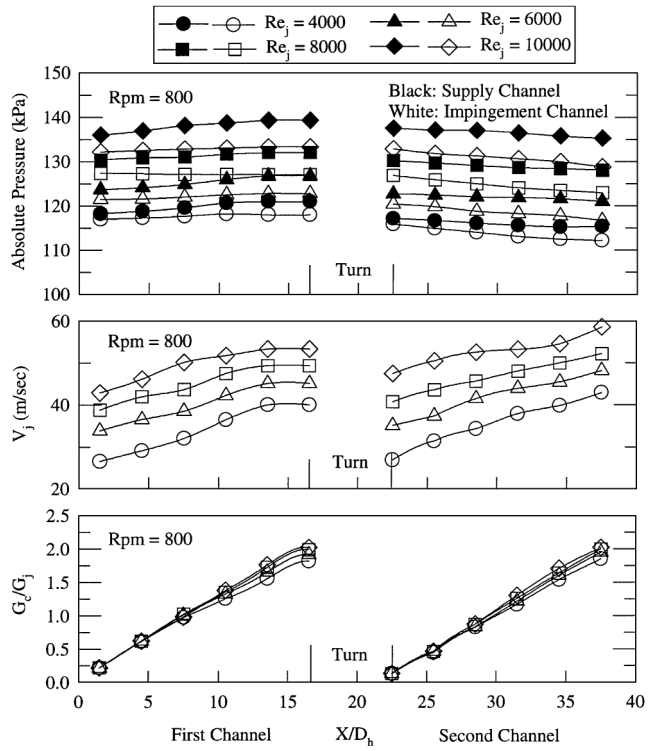

Fig. 4 Flow distribution for rotating test.

were maintained at around 52°C (125°F) for all Reynolds numbers and rotation speeds tested. The operating parameters Re_j and Ω together produced the following jet rotation numbers: $Ro = 0.0$, 0.0027, 0.0033, 0.0044, 0.0053, 0.0066, 0.0089, and 0.0133. The dimensionless parameters, such as Re_j, Ro, Z_n/d_j, e/D_h, and p/e, are in the range of gas turbine operation. The desired dimensionless parameters were achieved by enlarging the test model, which resulted in larger d_j and A_f and lower V_j, X_n/d_j, and Ω.

Figure 3 shows the flow distribution for the nonrotating test. The pressure levels in the supply and impingement channels, jet velocities, and ratios of channel spent air (crossflow) mass flux to jet mass flux increased with an increase in the jet Reynolds number. The channel crossflow mass flux at a given radial location is the sum of all impinging jet mass fluxes upstream of that radial location. Increasing X/D_h in both the first and second pass allows the following observations to be made: 1) The pressure in the supply channel increased. This may be because the mean flow velocity decreases toward the dead end of the supply channel. Therefore, the static pressure increases with X/D_h. 2) The pressure in the impingement channel decreased. 3) The pressure difference between the supply and impingement channel increased. Therefore, with increasing X/D_h, jet velocities and ratios of channel spent air (crossflow) mass flux to jet mass flux increased in both the first and second passes. The flow distribution was similar in both channels.

Figure 4 shows the flow distribution for the rotating test (800 rpm, forward rotation). Rotation-induced centrifugal force $\rho\Omega^2 r$ generated additional pressure forces in both the supply and the impingement channel. Force $\rho\Omega^2 r$ acted in the radially outward direction in both the first and the second passes. In the first pass, $\rho\Omega^2 r$ in the supply and impingement channel acted in the radially outward direction. This caused the pressure in the supply and impingement channel to increase in the radially outward direction. However, with increasing X/D_h, the pressure difference across the jet plate increased. Therefore, jet velocities and ratios of channel spent air mass flux to jet mass flux increased with increasing X/D_h.

In the second pass, $\rho\Omega^2 r$ in the supply and impingement channel acted in the radially outward direction. Force $\rho\Omega^2 r$ caused resistance to the movement of inward flow in the supply and impingement channel. This caused the pressure in the supply and impingement channel to decrease in the radially inward direction. However, the pressure difference between the supply and impingement channel still increased in the radially inward direction. Therefore, with increasing X/D_h, jet velocities and ratios of channel spent air mass flux to jet mass flux increased.

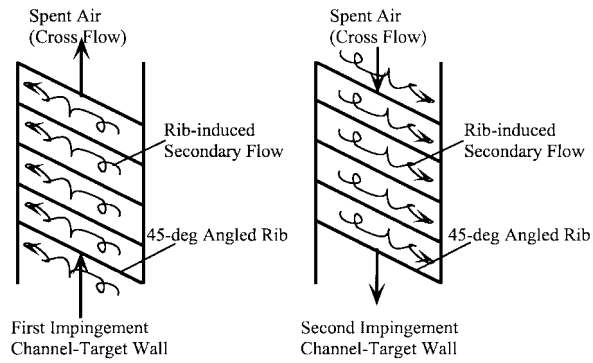

Fig. 5a Conceptual view of rib-induced secondary flow on nonrotating target walls.

Figure 5a shows the conceptual view of rib-induced secondary flow on nonrotating target walls. Angled ribs produced flow separation, flow reattachment, and also secondary flow between angled ribs on the walls. It is well known from previous investigations (for example, Han and Park[16]) that secondary flow enhanced turbulent mixing and reattachment reduced laminar sublayer thickness. This behavior changed the heat transfer distribution. The intensity of the secondary flow increased with an increase in spent air crossflow. The effect of rib-induced secondary flow on heat transfer distribution is shown in Fig. 6.

Figure 5b shows the conceptual view of flow and force distribution in rotating (forward rotation) impingement channels. A detailed description of flow behavior for forward and reverse rotation is given by Akella and Han.[12] A brief review on flow and force distribution is presented here. The jets traveled opposite to the direction of rotation in the first impingement channel. The channel Coriolis force pushed the cooler air toward the wall, which created mixing near the wall. However, the spent air crossflow, centrifugal force, and jet Coriolis force deflected the jets away and reduced the overall impingement

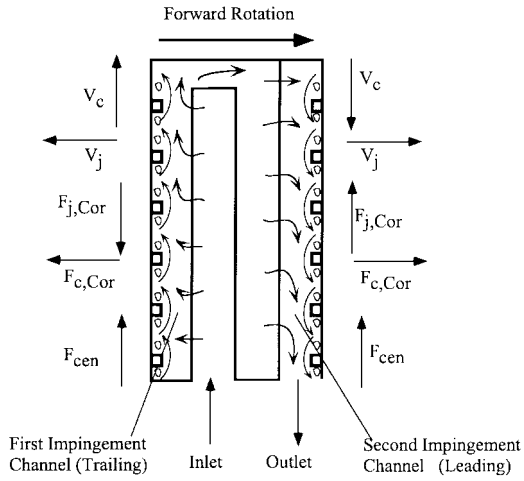

Fig. 5b Conceptual view of flow and force distribution in rotating impingement channels.

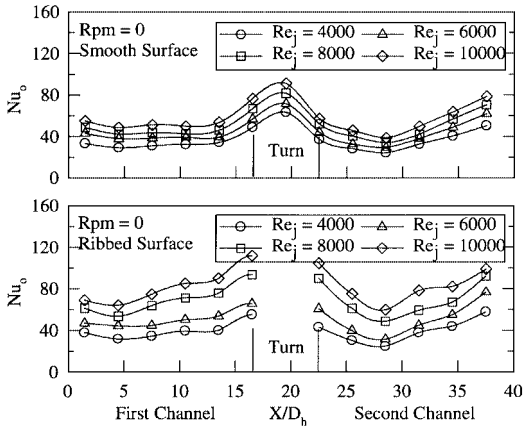

Fig. 6 Effect of angled ribs on nonrotating impingement heat transfer.

effect on the wall. The jets traveled in the direction of rotation in the second impingement channel. Again, the channel Coriolis force pushed the cooler air toward the wall and created higher velocity gradients near the wall. However, the overall impingement effect on the wall is reduced due to the defection of jets caused by the spent air crossflow, centrifugal force, and jet Coriolis force. It was qualitatively estimated that heat transfer is dominated by the impinging jets, and the effect of spent air crossflow and rotation are secondary as compared to impinging jets.

Figure 6 shows the effect of angled ribs on the Nusselt number distribution for the nonrotating test. Nusselt numbers on smooth surfaces are also provided to compare heat transfer behavior from ribbed surfaces with smooth surfaces. Akella and Han[12] performed experiments on smooth surfaces for similar test conditions. Heat transfer on smooth walls is briefly discussed. Nusselt numbers increased with an increase in jet Reynolds number. In the first impingement channel, both the jet velocity and spent air crossflow increased with an increase in X/D_h (Fig. 3). With an increasing X/D_h, the crossflow reduced the impingement effect, but the increased jet velocity compensated for the loss of heat transfer associated with crossflow. Therefore, the overall effect of the increasing crossflow and jet velocity resulted in relatively uniform Nusselt numbers on the smooth walls. High Nusselt number values are expected in the turn region due to a flow turning effect. In the second impingement channel, after the 180-deg turn, Nusselt number values decreased due to the spent air crossflow effect. Higher jet velocities toward the end of the channel resulted in higher Nusselt number values.

For the case of ribbed impingement channels, heat transfer values increased greatly with an increase in Reynolds numbers. Results showed that heat transfer from ribbed surfaces is higher when compared with those from smooth surfaces. This behavior is consistent with previous investigations of heat transfer enhancement. The jet and spent air velocities increased in both channels with increasing X/D_h (Fig. 3). For the radially outward flow, the Nusselt numbers increased from the inlet to the exit of the channel. Periodically placed 45-deg angled ribs generated flow separation, flow reattachment, and secondary flow between angled ribs on target walls (Fig. 5a), which resulted in reduced boundary-layer thickness, large velocity gradients, and increased mixing of air near the walls. The angled rib effect on heat transfer enhancement has been reported in a previous investigation.[16] The magnitude of velocity gradients increased with an increase in jet and spent air crossflow velocities, i.e., increased X/D_h or jet Reynolds numbers. Heat transfer values in the turn region are not reported because the temperature difference between the air and wall is small, which results in large uncertainties in the calculation of convection coefficients.

Nusselt numbers decreased from the turn region to the middle of the second channel for the radially inward flow. However, the Nusselt numbers increased from the middle to the exit of the channel. This may be because, near the entrance of the second channel (small X/D_h), the spent air crossflow could deflect the jets and reduce impingement effect. However, toward the exit of the channel (large X/D_h), the increased jet impinging velocities (Fig. 3) could enhance mixing and increase heat transfer; meanwhile, the increased spent air crossflow (Fig. 3) from the middle to the exit of the channel enhances rib-induced secondary flow mixing and increases heat transfer. Therefore, increasing heat transfer coefficients were recorded from the middle to the exit of the second channel.

Figure 7 shows the effect of rotation and angled ribs on impingement heat transfer. Nusselt numbers on smooth surfaces under rotation are also provided for similar test conditions. Nusselt numbers increased with an increase in Reynolds number. For smooth surfaces, the effect of rotation is to decrease the heat transfer compared to the nonrotation test (Fig. 7a vs Fig. 6a). Also, rotation decreased heat transfer for the ribbed surfaces compared to the nonrotating test (Fig. 7b vs Fig. 6b). Figure 5b showed that the channel Coriolis force pushed the cooler air toward the wall and enhanced the impingement effect on the wall. However, the spent air crossflow, centrifugal force, and jet Coriolis force deflected the jets away from the wall and reduced the overall impingement effect and heat transfer on the wall. Therefore, rotation reduced heat transfer in both smooth and ribbed impingement channels.

Angled ribs created flow separation, reattachment, and secondary flow between angled ribs (Fig. 5a), which enhanced the heat transfer from the walls. Although rotation reduced the jet impingement effect, the rib-induced turbulent mixing and secondary flow production greatly increased the heat transfer coefficients. Therefore, higher Nusselt numbers were recorded on ribbed walls compared to smooth walls for the rotation test (Fig. 7b vs Fig. 7a).

Figure 8 shows the effect of rotation on heat transfer in ribbed impingement channels. Results are presented for two rotation numbers

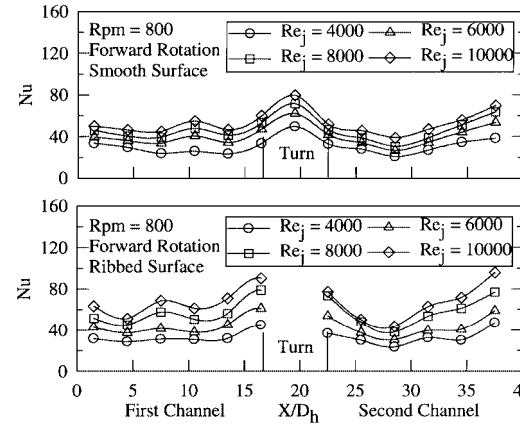

Fig. 7 Combined effect of rotation and angled ribs on impingement heat transfer.

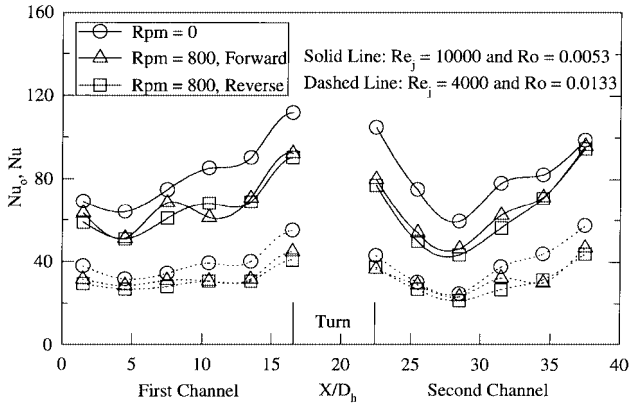

Fig. 8 Effect of rotation on Nusselt number distribution in ribbed channels.

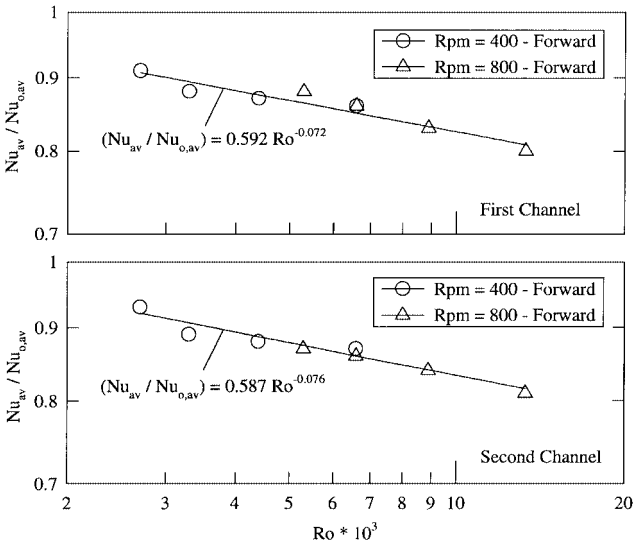

Fig. 9 Effect of rotation on ribbed channel-averaged Nusselt number ratio.

($Ro = 0.0053$ and 0.0133) and also for the nonrotating test. The effect of the jet direction with respect to the rotation direction is also observed (forward and reverse rotation). The jet traveled opposite to the direction of rotation in the first channel and in the same direction of rotation in the second channel for the forward rotation test. At a fixed Reynolds number, higher heat transfer values were recorded for the nonrotating test compared with those for the rotating test. Spent air, centrifugal force, and jet Coriolis force reduced the overall impingement effect in impingement channels during rotation test. Akella and Han[12] made two observations: 1) the channel Coriolis force $\rho\Omega V_c$ pushed the cooler air toward the target wall during forward rotation and 2) $\rho\Omega V_c$ pulled cooler air away from the target wall during reverse rotation. Therefore, reverse rotation had slightly lower heat transfer coefficients compared to forward rotation.

Figure 9 shows the ratio of rotation to nonrotation ribbed channel-averaged Nusselt numbers at various rotation numbers ($\Omega d_j / V_{j,\mathrm{av}}$). Ribbed channel-averaged Nusselt numbers (Nu_{av} for rotation, $Nu_{0,\mathrm{av}}$ for nonrotation) were based on an algebraic average of Nusselt number from six copper plates in each channel target wall. Rotation numbers varied from 0.0 to 0.0133. At a fixed rotation speed, a lower jet Reynolds number gave a large rotation number and, likewise, a higher jet Reynolds number gave a low rotation number. Rotation decreased Nusselt numbers up to 20%. The Nusselt number ratios decreased with an increase in rotation numbers. Correlations of the form $(Nu_{\mathrm{av}}/Nu_{0,\mathrm{av}}) = 0.592Ro^{-0.072}$ and $0.587Ro^{-0.076}$ represent the trends in the first and second impingement channels, respectively.

Figure 10 shows the effect of Reynolds numbers on ribbed channel-averaged Nusselt number values at various rotation speeds.

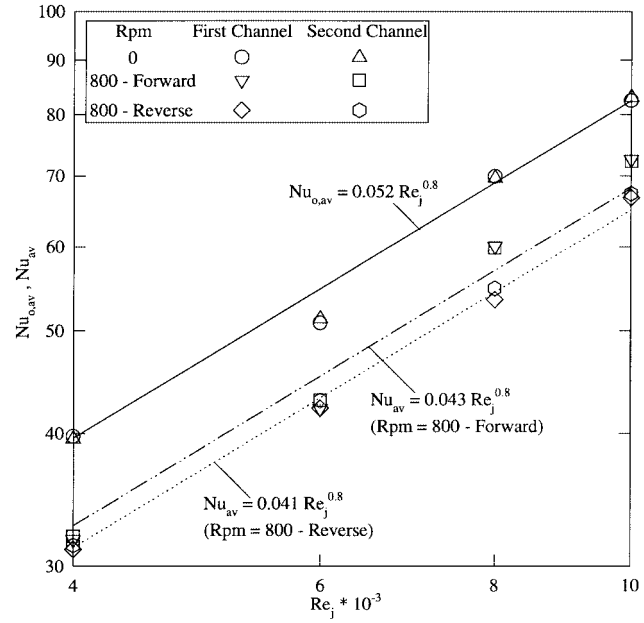

Fig. 10 Effect of Reynolds number on ribbed channel-averaged Nusselt number values at various rotation speeds.

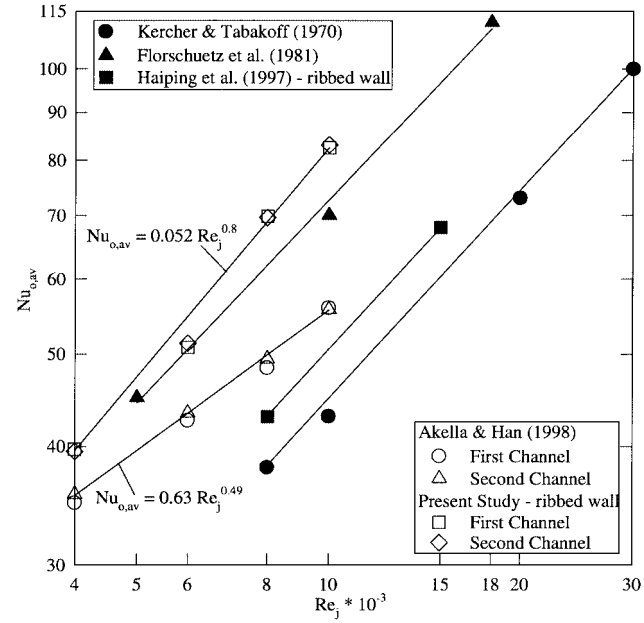

Fig. 11 Comparison of channel-averaged Nusselt number values with previous studies for nonrotating test.

A least-square curve fit was performed and correlations of the form $Nu_{0,\mathrm{av}} = 0.052Re_j^{0.8}$, $Nu_{\mathrm{av}} = 0.043Re_j^{0.8}$, and $Nu_{\mathrm{av}} = 0.041Re_j^{0.8}$ were developed for the nonrotating, forward rotating, and reverse rotating tests, respectively. Reverse rotation decreased heat transfer values by 20% in the impingement channels at $Re_j = 1 \times 10^4$.

Figure 11 compares the results obtained from current investigation (ribbed walls for nonrotating test) with previous nonrotating studies. The current investigation was conducted for fixed geometric parameters, such as $d_j = 3.18$ mm, $X_n/d_j = 2$, $Y_n/d_j = 3$, $Z_n/d_j = 3$, $A_f = 12\%$, $\alpha = 45$ deg, $p/e = 10$, and $e/D_h = 0.125$. Kercher and Tabakoff,[1] Akella and Han,[12] and Florschuetz et al.[3] obtained heat transfer coefficients on smooth surfaces for different geometric and flow parameters. For the case of smooth surfaces, at $Re_j = 1 \times 10^4$, the heat transfer values measured by Akella and Han[12] are 30% higher and 20% lower when compared with Kercher and Tabakoff[1] and Florschuetz et al.,[3] respectively. Florschuetz et al.[3] obtained heat transfer values for a minimum

crossflow scheme. This is why the Florschuetz et al.[3] data are higher. They presented a correlation for jet impingement with minimum crossflow for inline and staggered rows of jets. Kercher and Tabakoff[1] measured heat transfer coefficients for $d_j = 2.01$ mm, $X_n/d_j = 6.25$, $Y_n/d_j = 6.25$, $Z_n/d_j = 1$, $A_f = 2\%$, and maximum crossflow scheme. Akella and Han[12] provided more cooling spots on the walls ($A_f = 12\%$), which resulted in higher velocity gradients and high heat transfer values compared with Kercher and Tabakoff[1] ($A_f = 2\%$).

For the case of ribbed surface, Haiping et al.[8] measured heat transfer coefficients under a maximum crossflow scheme for different geometric and flow parameters. They measured heat transfer values for the following parameters: $X_n/d_j = 10$, $Y_n/d_j = 10$, $Z_n/d_j = 3$, $A_f = 0.8\%$, $\alpha = 90$ deg, and $p/e = 10$. At $Re_j = 1 \times 10^4$, the Nusselt number from the current study (ribbed surfaces) is 59% higher than Haiping et al.[8] Previous studies[13,14] concluded that 90-deg ribs provide lower heat transfer coefficients when compared with angled ribs. Also, the current study (ribbed surfaces) has more cooling spots ($A_f = 12\%$) compared to Haiping et al.[8] ($A_f = 0.8\%$). The presence of more cooling spots and secondary flow induced by 45-deg angled ribs enhanced the mixing of air and velocity gradients near the walls. This resulted in higher Nusselt number values for the current investigation than for Haiping et al.[8]

Finally, results from the current study (ribbed walls) are compared with those from Akella and Han.[12] Periodically placed angled ribs (45 deg) created flow separation, flow reattachment, and induced secondary flow between angled ribs on target walls.[16] This resulted in increased turbulent mixing of air near the walls. Therefore, jet impingement on angled ribbed walls produced more heat transfer compared to jet impingement on smooth walls (Fig. 6b). Figure 11 shows that Nusselt number from the current study (ribbed walls) is 47% higher when compared with Akella and Han,[12] at $Re_j = 1 \times 10^4$ for the nonrotating case. The angled rib effect on the impingement heat transfer increased with an increase in jet Reynolds number.

Figure 12 shows the effect of Reynolds numbers on rib to smooth heat transfer enhancement ratios at various rotation speeds. The channel-averaged Nusselt numbers from this study (ribbed walls) were compared with those from Akella and Han[12] (smooth walls). Similar test conditions were maintained for the smooth and ribbed surfaces. As the jet Reynolds number increased from 4×10^3 to 1×10^4, the heat transfer enhancement ratio increased from 13 to 47% for the nonrotating test. Because of the rotation effect, however, these enhancement ratios changed from 9 to 44% as the jet Reynolds number increased. This implies that the angled rib effect still dominates the near-wall flowfield and heat transfer behavior, regardless of whether the effect of rotation would reduce heat transfer enhancement ratios. It is observed that the enhancement ratios increased gradually for lower jet Reynolds numbers ($Re_j < 6 \times 10^3$). This is because the rib-induced turbulence effect is small for the lower spent air crossflow. But the enhancement ratios increased sharply for $Re_j > 6 \times 10^3$. Rib-induced secondary flow promoted turbulent mixing of air near the walls, and this behavior increased the heat transfer rate. The intensity of secondary flow increased with an increase in the spent air crossflow (related to jet Reynolds number). However, further increasing the jet Reynolds numbers causes the slope of the enhancement ratios to slow down. This may be because the heat transfer rates are already pretty high at the higher jet Reynolds numbers; therefore, the angled rib has reached its maximum effect on enhancing jet impingement heat transfer. Note that for ribbed walls the rib increased surface area is about 28% and is not included in the calculation of the heat transfer coefficient.

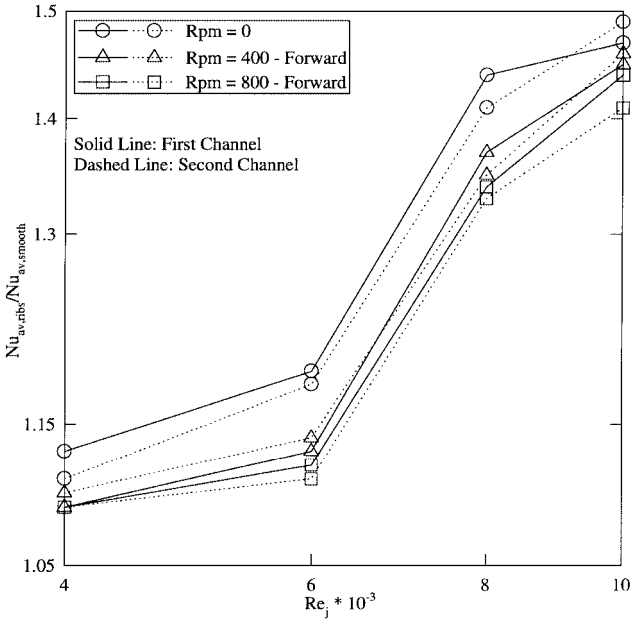

Fig. 12 Effect of Reynolds number on rib to smooth heat transfer enhancement ratios at various rotation speeds.

Conclusions

This study investigated the following issues on impingement heat transfer: 1) the effect of angled ribs in nonrotating impingement-cooled blades and 2) the combined effect of rotation and angled ribs in rotating impingement-cooled blades. Measurements were obtained in a two-pass rectangular impingement channel, with the channels connected by a sharp 180° turn. Square cross-sectioned ribs with a rib-orientation angle of 45 deg were periodically attached to the walls. The effect of the jet direction with respect to the rotation direction was also studied. Secondary flows produced by angled ribs and rotation interacted with each other and developed a new heat transfer pattern that is different from those produced by angled ribs or by rotation alone. The main conclusions follow.

1) The rotation-induced centrifugal force $\rho\Omega^2 r$ increased pressure levels when compared with those for the nonrotating test. However, the jet velocity distributions did not change significantly when compared with those for the nonrotating test.

2) For the rotating test, the overall impingement effect on the wall reduced due to the defection of jets caused by the centrifugal force and jet Coriolis force. Therefore, lower heat transfer coefficients were recorded during rotation compared with the values obtained for the nonrotating tests.

3) As the jet Reynolds number increased from 4×10^3 to 1×10^4, the rib to smooth heat transfer enhancement ratios increased from 13 to 47% for the nonrotating test. This is due to the effect of flow separation, reattachment, and secondary flow generated by impinging jets over angled ribs.

4) For the rotating test (800 rpm, forward rotation), the rib to smooth heat transfer enhancement ratios changed from 9 to 44% as the jet Reynolds number increased from 4×10^3 to 1×10^4. This is because rotation reduces the enhancement effect produced by impinging jets over angled ribs.

5) Rotation decreased heat transfer coefficients up to 20% on the ribbed walls. The rotation to nonrotation Nusselt number ratios decreased with an increase in rotation numbers. Correlations of the form $(Nu_{av}/Nu_{0,av}) = 0.592Ro^{-0.072}$ and $0.587Ro^{-0.076}$ represent the trends in the first and second impingement channels, respectively.

6) The rib to smooth heat transfer enhancement ratios in the first impingement channel are slightly higher when compared with those in the second impingement channel.

7) Ribbed channel-averaged Nusselt number values for the forward rotation test are slightly higher when compared with those for the reverse rotation test.

Acknowledgments

This paper was prepared with the support of the U.S. Department of Energy, Morgantown Energy Technology Center, Cooperative Agreement DE-FC21-92MC9061. The project was also supported by the Texas Higher Education Coordinating Board Advanced Technology Program under Grant 999903-165 (TEES 32190-71720 ME). Their support is greatly appreciated.

References

[1] Kercher, D. M., and Tabakoff, W., "Heat Transfer by a Square Array of Round Air Jets Impinging Perpendicular to a Flat Surface Including the

Effect of Spent Air," *Journal of Engineering for Power*, Vol. 92, No. 1, 1970, pp. 73–82.

[2]Chance, J. L., "Experimental Investigation of Air Impingement Heat Transfer Under an Array of Round Jets," *TAPPI*, Vol. 57, No. 6, 1974, pp. 108–112.

[3]Florschuetz, L. W., Truman, C. R., and Metzger, D. E., "Streamwise Flow and Heat Transfer Distributions for Jet Array Impingement with Cross Flow," *Journal of Heat Transfer*, Vol. 103, No. 2, 1981, pp. 337–342.

[4]Van Treuren, K. W., Wang, Z., Ireland, P. T., and Jones, T. V., "Detailed Measurements of Local Heat Transfer Coefficient and Adiabatic Wall Temperature Beneath an Array of Impinging Jets," *Journal of Turbomachinery*, Vol. 116, No. 2, 1994, pp. 369–374.

[5]Huang, Y., Ekkad, S., and Han, J. C., "Detailed Heat Transfer Distribution Under an Array of Orthogonally Impinging Jets," *Journal of Thermophysics and Heat Transfer*, Vol. 12, No. 1, 1998, pp. 73–79.

[6]Trabold, T. A., and Obot, N. T., "Impingement Heat Transfer Within Arrays of Circular Jets: Part 2—Effects of Cross Flow in the Presence of Roughness Elements," *Journal of Turbomachinery*, Vol. 109, No. 4, 1987, pp. 594–601.

[7]Gau, C., and Lee, C. C., "Impingement Cooling Flow Structure and Heat Transfer Along Rib-Roughened Walls," *International Journal of Heat and Mass Transfer*, Vol. 35, No. 11, 1992, pp. 3009–3020.

[8]Haiping, C., Dalin, Z., and Taiping, H., "Impingement Heat Transfer from Rib Roughened Surface Within Arrays of Circular Jet: The Effect of the Relative Position of the Jet Hole to the Ribs," *International Gas Turbine and Aeroengine Congress and Exhibition*, American Society of Mechanical Engineers, New York, 1997.

[9]Epstein, A. H., Kerrebrock, J. L., Koo, J. J., and Preiser, U. Z., "Rotational Effects on Impingement Cooling," Gas Turbine Lab., Rept. 184, Massachusetts Inst. of Technology, Cambridge, MA, Sept. 1985.

[10]Mattern, C., and Hennecke, D. K., "The Influence of Rotation on Impingement Cooling," *TurboExpo*, American Society of Mechanical Engineers, New York, 1996.

[11]Parsons, J. A., Han, J. C., and Lee, C. P., "Rotation Effect on Jet Impingement Heat Transfer in Smooth Rectangular Channels with Four Heated Walls and Radially Outward Cross Flow," *Journal of Turbomachinery*, Vol. 120, No. 1, 1998, pp. 79–85.

[12]Akella, K. V., and Han, J. C., "Jet Impingement Cooling in Rotating Two-Pass Rectangular Channels with Smooth Walls," *Journal of Thermophysics and Heat Transfer*, Vol. 12, No. 4, 1998, pp. 582–588.

[13]Johnson, B. V., Wagner, J. H., Steuber, G. D., and Yeh, F. C., "Heat Transfer in Rotating Serpentine Passages with Trips Skewed to the Flow," *Journal of Turbomachinery*, Vol. 116, No. 1, 1994, pp. 113–123.

[14]Zhang, Y. M., Han, J. C., Parsons, J. A., and Lee, C. P., "Surface Heating Effect on Local Heat Transfer in a Rotating Two-Pass Square Channel with 60 deg Angled Rib Turbulators," *Journal of Turbomachinery*, Vol. 117, No. 2, 1995, pp. 272–280.

[15]Kline, S. J., and McClintock, F. A., "Describing Uncertainties in Single-Sample Experiments," *Mechanical Engineering*, Vol. 75, No. 1, 1953, pp. 3–8.

[16]Han, J. C., and Park, J. S., "Developing Heat Transfer in Rectangular Channels with Rib Turbulators," *International Journal of Heat and Mass Transfer*, Vol. 31, No. 1, 1988, pp. 183–195.